(Received 15 October 2025, Accepted 30 December 2025, Scheduled 16 January 2026)

An Asymmetric Miniaturized Single-Layer Bandpass Filter Based on Interdigital Capacitors and Microstrip Inductors

Juntao Cao[1,2], Xiaoying Zuo[1,2,*], Mengxin He[1,2], Yajian Li[1,2], and Jiapei Dong[1,2]

[1]*Laboratory for Sensor, Beijing Information Science & Technology University, Beijing 100192, China*
[2]*School of Applied Science, Beijing Information Science & Technology University, Beijing 100192, China*

ABSTRACT: This paper proposes an asymmetric miniaturized single-layer bandpass filter based on interdigital capacitors and microstrip inductors with miniaturization and a wide bandwidth. It is composed of three series of LC resonator pairs and two parallel LC resonator pairs, and this asymmetric structure enhances design flexibility. The measured results indicate that the center frequency is 1.48 GHz, and the passband covers $0.88 \sim 2.08$ GHz, with a return loss better than 12.6 dB, whereas the insertion loss is less than 0.58 dB. The physical size is 31 mm $\times$13 mm, which is smaller than that of traditional LC filters.

1. INTRODUCTION

With the rapid development of wireless communication systems, filters based on interdigital capacitors and microstrip inductors have become a research hotspot. In [1], a switchable bandpass filter based on interdigital capacitors and microstrip inductors is proposed. It realizes single/double band switching through PIN diodes with independently controllable transmission zeros and a compact structure. In [2], a broadband filter based on interdigital capacitors and microstrip inductors is proposed, achieving a 38.9% 3-dB relative bandwidth and high selectivity with advantages of miniaturization and easy integration. For high-precision, multi-functional electromagnetic detection in wireless communication, traditional single-function devices lack sufficient sensitivity. Second harmonic generation (SHG) with frequency doubling and functional materials like graphene/liquid crystals enables breakthroughs, as shown in Yang et al. innovative studies [3, 4].

In [5], a hybrid filter combining a quasi-lumped-element filtering network and $LiNbO_3$/SiC SAW resonators is proposed to overcome the narrow bandwidths of traditional acoustic filters. Cross-coupling/hybrid coupling-based transmission zero schemes are complex and sensitive to the manufacturing precision. To address this, cascade lumped elements (capacitors/inductors) in transmission lines. This allows resonators to gain adjustable anti-resonant frequencies, generating $N, 2N$ [6] or $3N + 1$ [7] near-passband transmission zeros without complex coupling. In [8], a universal synthesis method is proposed to address the difficult negative coupling implementation and excessive reliance on optimization. It converts coupling forms via similarity transformation, enabling direct lumped-component implementation without optimization and supporting multiple transmission zeros and a measured 70.5% fractional bandwidth (FBW). A cubic miniaturized filter with quasi-TM_{010} mode dielectric-loaded cavities is proposed in [9], balancing performance and miniaturization to solve the large size of traditional cavity/waveguide filters that fail at compact integration of wireless devices. A scaled metal waveguide filter via metamaterial resonators and 3D printing is proposed in [10], which achieves effective size reduction to adapt to compact radio frequency front-ends.

The bandpass filter proposed in this paper consists of interdigital capacitors and microstrip inductors. This filter is intended to be used in a wearable positioning system. The operating frequency band of the positioning system is $1710 \sim 1880$ MHz, so the filter has a center frequency of 1.48 GHz. Its passband covers $0.88 \sim 2.08$ GHz, with return loss better than 12.6 dB and insertion loss less than 0.58 dB.

2. THEORETICAL ANALYSIS

2.1. Circuit Topology and Parameter Optimization

Figure 1 presents the circuit topology of the proposed bandpass filter, which consists of five capacitors and five inductors with an asymmetric configuration. This asymmetric LC topology enhances the flexibility of miniaturized design without a strict symmetric layout. The circuit parameters are optimized through electromagnetic simulation, and the values are determined as follows: $C_1 = 1.71$ pF, $C_2 = 9.51$ pF, $C_3 = 2.01$ pF, $L_1 = 7.03$ nH, $L_2 = 2.76$ nH, $L_3 = 7.71$ nH. Z_0 is the terminal impedance and is set to 50 Ω. The ideal simulated S-

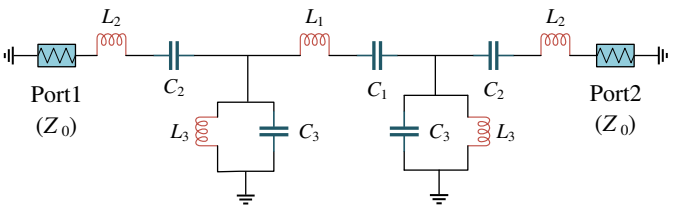

FIGURE 1. Schematic diagram of bandpass filter circuit.

* Corresponding author: Xiaoying Zuo (zuoxiaoying03@163.com).

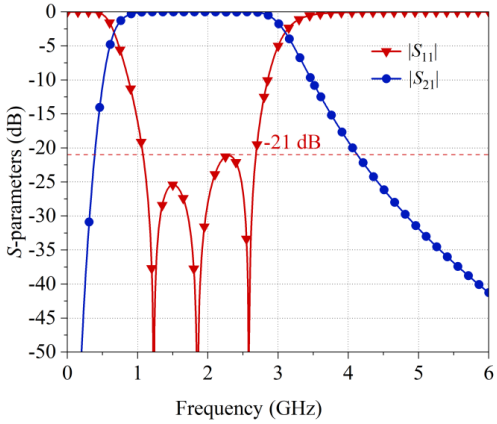

FIGURE 2. Ideal simulated S-parameters of the bandpass filter.

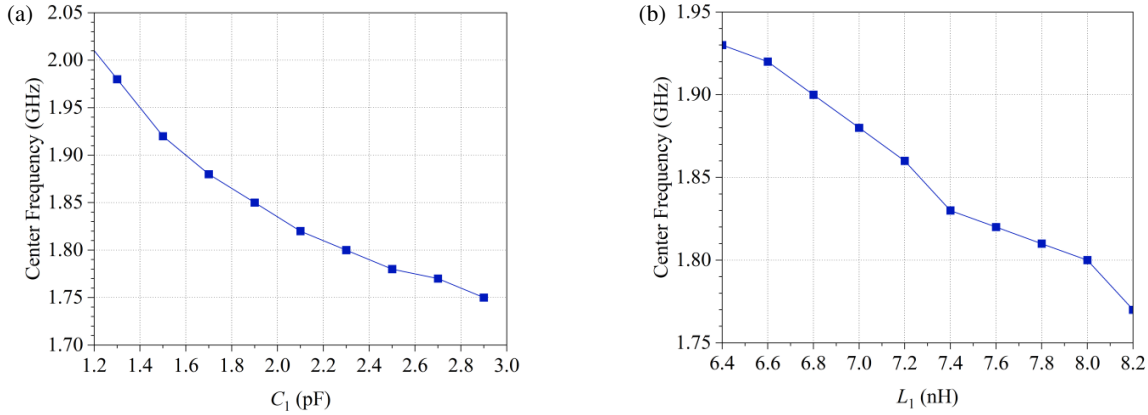

FIGURE 3. (a) The center frequency varies with the values of (a) C_1 and (b) L_1.

parameters of the circuit schematic are shown in Fig. 2. The return loss across the entire passband reaches 21 dB. This result verifies the rationality of the proposed circuit topology and the optimized parameter values.

2.2. Key Performance Parameters and Analysis of Parameter Influence

The core performance parameters of the bandpass filter, including the center frequency (f_0), 3 dB absolute bandwidth (BW), 3 dB relative bandwidth (FBW), and quality factor (Q) [11], are defined by the following formulas:

$$f_0 = \frac{f_1 + f_2}{2} \tag{1}$$

$$\text{BW} = f_2 - f_1 \tag{2}$$

$$\text{FBW} = \frac{\text{BW}}{f_0} \tag{3}$$

$$Q = \frac{f_0}{\text{BW}} \tag{4}$$

where f_1 and f_2 are the lower and upper 3 dB cutoff frequencies of the passband, respectively. Formulas (3) and (4) indicate that the 3 dB relative bandwidth is inversely proportional to the quality factor. This relationship provides a theoretical basis for parameter adjustment during the filter design process [12].

Figure 3(a) illustrates the variation in the center frequency with capacitor C_1. The center frequency decreases gradually as the capacitance of C_1 increases. Similarly, Fig. 3(b) shows that the center frequency exhibits a decreasing trend with the increase of inductance. Figs. 4(a) and (b) depict the variations of 3 dB relative bandwidth and quality factor with C_3 and L_3, respectively. As shown in Fig. 4(a), with the increase of C_3, the 3 dB relative bandwidth decreases while the quality factor increases. Conversely, Fig. 4(b) indicates that as L_3 increases, the 3 dB relative bandwidth also decreases, and the quality factor increases. These results further validate the inverse proportional relationship between FBW and Q, and demonstrate that C_3 and L_3 are key parameters for adjusting the bandwidth and selectivity of the filter.

Transmission poles (TPs) are crucial for improving the selectivity of the bandpass filter [13]. Fig. 5 shows that there are three transmission poles in the proposed filter, which are sequentially labeled as TP1, TP2, and TP3, located at 1.23 GHz, 1.86 GHz, and 2.58 GHz, respectively. Figs. 5(a) and (b) reveal that the positions of the transmission poles vary with the values of C_3 and L_3. Specifically, the adjustment of C_3 and L_3 can shift the transmission poles, thereby optimizing the passband flatness and out-of-band rejection performance of the fil-

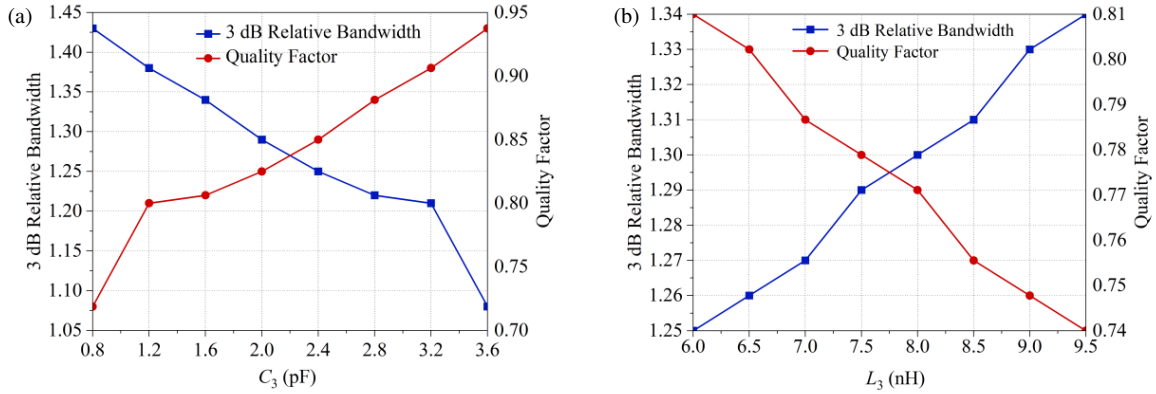

FIGURE 4. 3 dB relative bandwidth and quality factor vary with the values of (a) C_3 and (b) L_3.

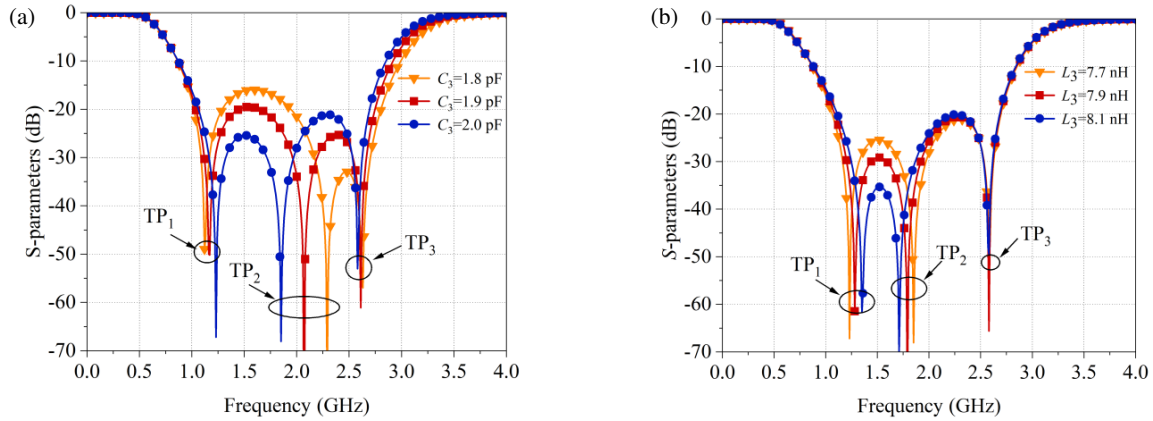

FIGURE 5. The position of transmission pole varies with the values of (a) C_3 and (b) L_3.

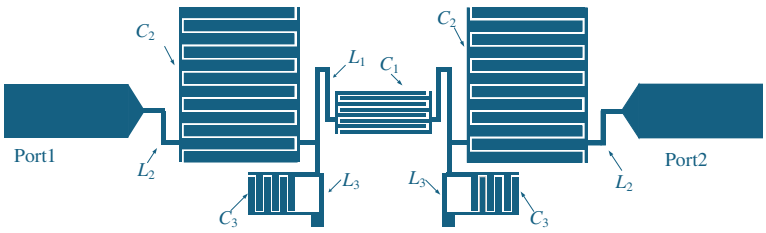

FIGURE 6. The layout of the bandpass filter.

ter [14]. Based on the measured simulation results, the lower cutoff frequency f_1 of 0.88 GHz and an upper cutoff frequency f_2 of 2.08 GHz are obtained. Substituting these values into formula (1), the center frequency $f_0 = 1.48$ GHz is calculated. Furthermore, the 3 dB absolute bandwidth is 1.2 GHz, and the 3 dB relative bandwidth (FBW) is 81.1% [15]. The compact LC structure has significantly reduced the size.

3. FILTER DESIGN

The bandpass filter employs interdigital capacitors and microstrip inductors as core structures. Among them, interdigital capacitors feature low parasitic parameters, whereas microstrip inductors balance integration and inductance needs with a meander line. A series LC resonance enables efficient signal transmission, and parallel LC resonance suppresses out-of-band interference. Measurements show the filter exhibits excellent performance: insertion loss is less than 0.58 dB and $|S_{11}|$ is better than 12.6 dB. This performance satisfies the signal gating requirements of wireless communication systems.

3.1. Design of Interdigital Capacitors and Microstrip Inductors

Figure 6 shows the filter layout. Fig. 7 shows that the capacitance of the interdigital capacitors varies with the structural parameters. The core structural parameters of the interdigital capacitor (L_a, W_a, G, N) are schematically depicted in Fig. 8(a). Specifically, Figs. 7(a), (b), and (d) show that the capacitance increases with the key parameters: finger length (L_a), finger width (W_a), and finger number (N). In contrast, Fig. 7(c) indicates that the capacitance decreases as the interdigital gap (G)

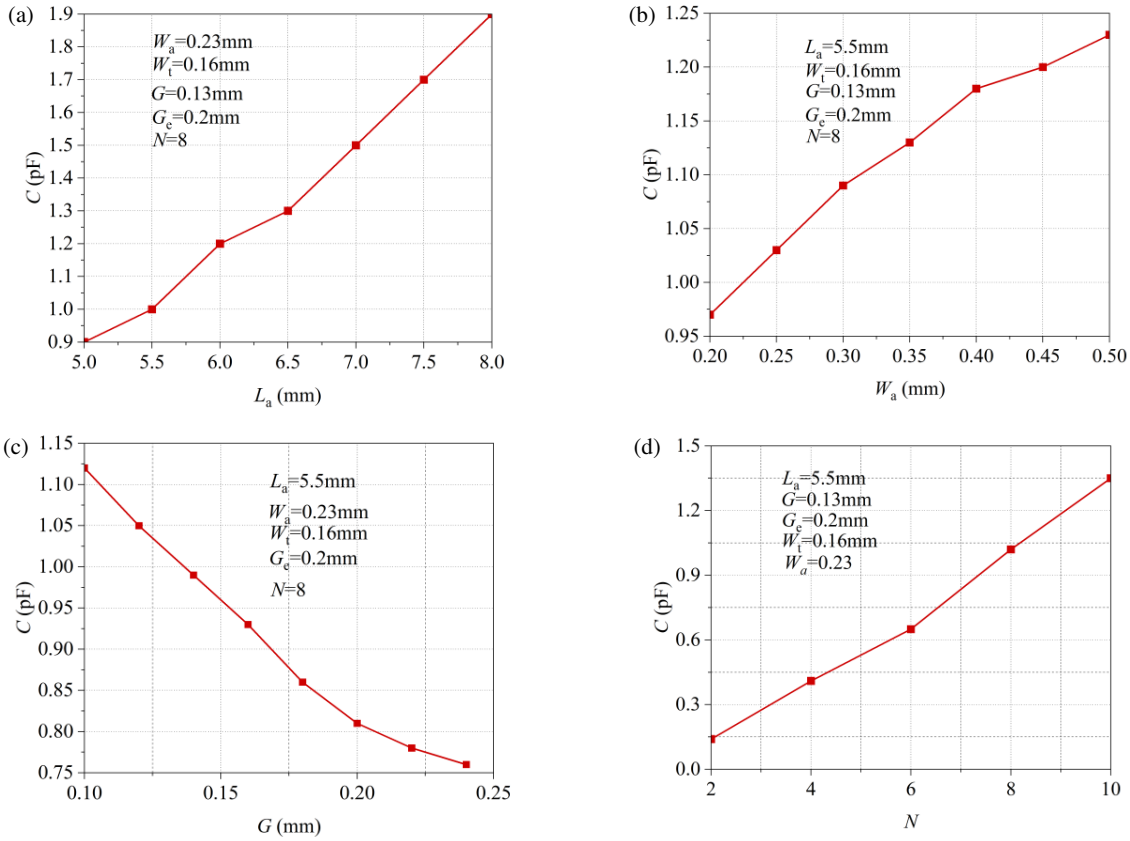

FIGURE 7. The capacitance value of interdigital capacitors varies with the values of (a) L_a, (b) W_a, (c) G, and (d) N.

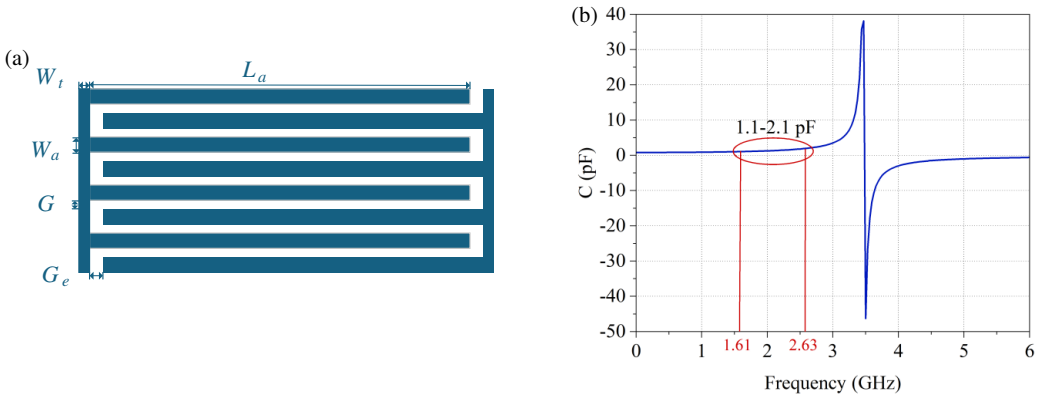

FIGURE 8. The layout of (a) interdigital capacitor and (b) the extracted capacitance value of the interdigital capacitor.

increases. Fig. 8(b) shows the capacitance variation with increasing frequency. An electromagnetic simulation of the interdigital capacitor structure is conducted, and the capacitance value is extracted using formula (5). Fig. 9(a) shows the layout structure of the microstrip inductor. Here, L_b represents the length of the microstrip inductor, and W_b denotes its width. Fig. 9(b) shows the inductance variation achieved by adjusting L_b and W_b. An electromagnetic simulation is also performed for the microstrip inductor structure, with inductance extraction using formula (6). Formulas (5) and (6) are referenced from [2].

$$C = -\frac{\mathrm{Im}(Y_{12})}{2\pi f} \tag{5}$$

$$L = -\frac{1}{2\pi f \mathrm{Im}(Y_{11})} \tag{6}$$

3.2. Simulation and Measurement

This paper selects Rogers RO4350B as the substrate, with relative dielectric constant $r = 3.66$, loss tangent $\delta = 0.0037$, thickness $h = 1.524$ mm, and copper foil thickness of 0.035 mm. The layout structure is composed of interdigital capacitors and microstrip inductors. Iterative optimization is performed on key parameters: for interdigital capacitors, these include the interdigital gap, finger length, finger width, and

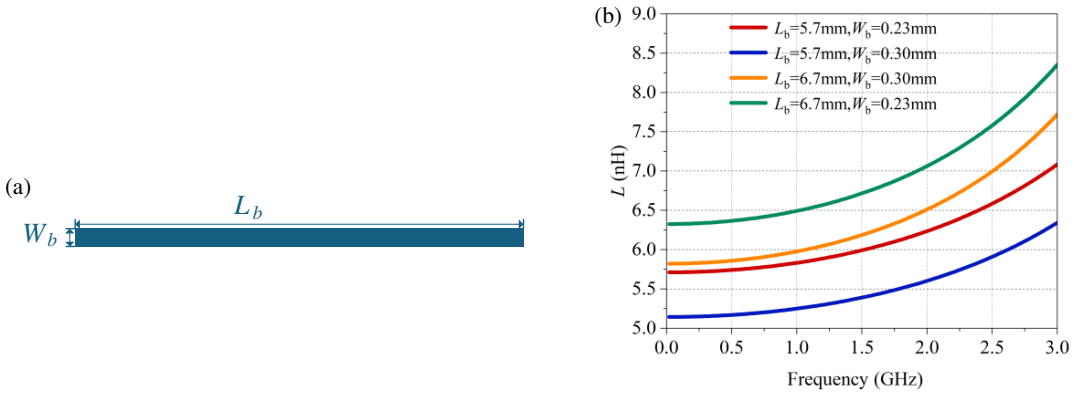

FIGURE 9. The layout of (a) microstrip inductor and (b) the inductance value of the extracted microstrip inductor.

TABLE 1. Structural parameters of the interdigital capacitor (unit: mm).

Capacitor	N	W	L	G	G_e	W_t
C_1	8	0.23	5.5	0.13	0.2	0.16
C_2	12	0.65	7.1	0.2	0.2	0.13
C_3	6	0.4	2.2	0.13	0.13	0.13

TABLE 2. Comparison of filter performance.

Filter Structures	Center Frequencies (GHz)	Insertion Loss (dB)	Return Loss (dB)	3 dB Relative Bandwidth (%)	Physical Dimensions ($\lambda g \times \lambda g$)
Ref. [2]	4.52	1.68	21.5	38.9	0.31×0.21
Ref. [5]	3.62	1.48	-	27.0	0.07×0.06
Ref. [8]	1.22	0.69	12.0	70.5	0.13×0.06
Ref. [13]	1.25	0.90	14.5	62.4	0.23×0.13
This work	**1.48**	**0.58**	**12.6**	**81.1**	**0.24×0.10**

finger number; for microstrip inductors, the line width and length are optimized. The core circuit size is $0.24\lambda_g \times 0.10\lambda_g$ (31 mm $\times$ 13 mm), (λ_g: the guided wavelength at the center frequency).

The simulated and measured performance metrics are shown in Fig. 10, Fig. 11 shows the layout simulation results of different interdigital gaps, and a photograph of the filter is shown in Fig. 12. Fig. 10 shows the simulation results of the LC layout, which are largely consistent with the schematic simulation. In the passband, the simulated return loss reaches 20.9 dB, and the insertion loss is less than 0.58 dB. Table 1 lists the structural parameters of the interdigital capacitor, where N, W, L, G, G_e, and W_t represent the finger count, line width, finger length, interdigital gap, finger end gap, and terminating microstrip width, respectively.

Table 2 lists the filter performance comparison with other designs. Discrepancies in passband return loss between simulation and measurement are caused by machining accuracy and transmission line loss during actual testing. We perform a tolerance analysis (or sensitivity analysis) in ADS. When the interdigital gap G of the interdigital capacitor C_2 is 0.15 mm, the simulation result is shown in Fig. 11(a). When the value of G is adjusted to 0.13 mm, the simulation result is shown in Fig. 11(b). Such a slight adjustment will cause the deterioration of the return loss in the passband, and insufficient processing accuracy will easily lead to differences between the layout and the measured results.

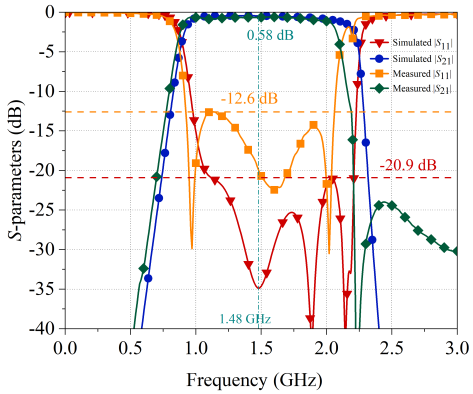

FIGURE 10. Simulated and measured results of the bandpass filter.

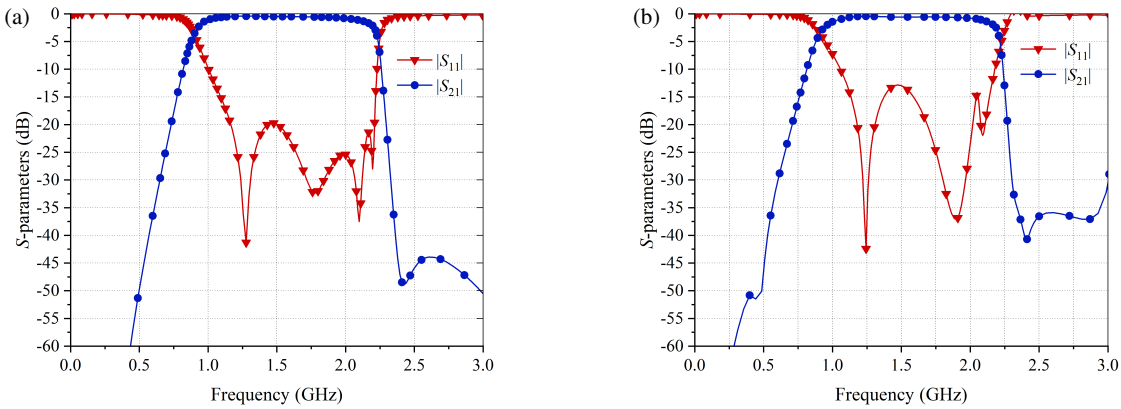

FIGURE 11. Layout simulation results.

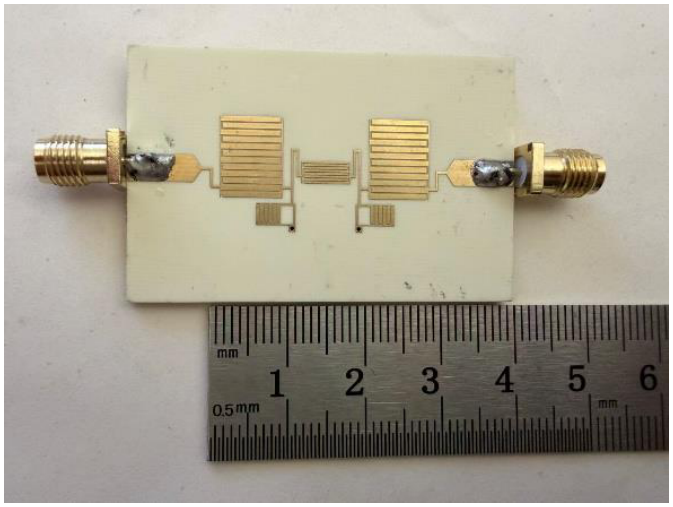

FIGURE 12. Physical image of filter processing.

4. CONCLUSION

This paper proposes a miniaturized, low-cost single-layer bandpass filter based on interdigital capacitors and microstrip inductors. It features miniaturization, low insertion loss, and an excellent overall performance. The schematic design, layout structure, and physical prototype of the filter are detailed in this paper. Comprehensive electromagnetic simulations and experimental measurements have further validated its reliable performance.

ACKNOWLEDGEMENT

This work was supported by the National Natural Science Foundation of China (62201065).

REFERENCES

[1] Mu, R., Y. Wu, L. Pan, W. Zhao, and W. Wang, "A miniaturized low-loss switchable single-and dual-band bandpass filter," *International Journal of RF and Microwave Computer-Aided Engineering*, Vol. 2023, No. 1, 9025980, 2023.

[2] Zhang, W., Y. Wu, W.-M. Wang, L.-W. Hao, and Y.-H. Yang, "A novel single-layer low-cost broadband bandpass filter based on interdigital capacitors and microstrip inductors," *Acta Electronica Sinica*, Vol. 51, No. 6, 1413–1420, 2023.

[3] Yang, C., C.-M. Guo, J. Xu, and H.-F. Zhang, "Device design for multitask graphene electromagnetic detection based on second harmonic generation," *IEEE Transactions on Microwave Theory and Techniques*, Vol. 72, No. 7, 4174–4182, 2024.

[4] Yang, C., C.-M. Guo, Y.-X. Wei, and H.-F. Zhang, "Electromagnetic detection design in liquid crystals Janus metastructures based on second harmonic generation," *IEEE Transactions on Instrumentation and Measurement*, Vol. 73, 1–11, 2024.

[5] Zhang, J., M. Sun, J.-X. Xu, X. Yao, S. Zhang, X. Ou, and X. Y. Zhang, "Compact wideband high-selectivity bandpass filter based on hybrid design of quasi-lumped-element filtering network and $LiNbO_3$/SiC SAW resonators," *IEEE Transactions on Microwave Theory and Techniques*, Vol. 73, No. 10, 7884–7894, 2025.

[6] Zakharov, A. V. and S. M. Litvintsev, "Lumped-distributed resonators providing N or 2N transmission zeros at real frequencies in bandpass filters without cross and mixed couplings," *IEEE Transactions on Microwave Theory and Techniques*, Vol. 72, No. 6, 3682–3691, 2024.

[7] Zakharov, A. V. and S. M. Litvintsev, "Lumped-distributed resonators providing multiple transmission zeros in bandpass filters with simple and mixed couplings," *IEEE Transactions on Circuits and Systems I: Regular Papers*, Vol. 71, No. 8, 3502–3513, 2024.

[8] Liu, B., K. Li, X. Chen, P.-L. Chi, and T. Yang, "Synthesis of wideband bandpass filter with cross-coupled or inline topology for direct circuit implementation using lumped elements," *IEEE Transactions on Microwave Theory and Techniques*, Vol. 72, No. 1, 737–749, 2024.

[9] Zeng, L.-X. and F.-M. Lin, "Miniaturized high-performance cube-shaped filter made up of quasi-TM_{010} mode dielectric-loaded cavities," *IEEE Access*, Vol. 8, 847–855, 2019.

[10] Cho, J., Y. Seo, J. Cho, K. Y. Park, J. Park, H. Lee, and S. Kahng, "Effective size reduction of the metallic waveguide bandpass filter with metamaterial resonators and its 3D-printed version," *Sensors*, Vol. 23, No. 3, 1173, 2023.

[11] Nie, H., B. Lan, T. Yu, D. Liu, X. Yu, Q. J. Gu, and Z. Xu, "A 1.3–1.7-GHz Q-enhanced resonator-based high-IF bandpass filter with 1.5%–67% tunable fractional bandwidth in 65-nm CMOS process," *IEEE Transactions on Microwave Theory and Techniques*, Vol. 72, No. 7, 4028–4042, 2024.

[12] Wang, H., N. An, S. Li, H. Zhao, and X. Yin, "A miniaturized interdigital bandpass filter with capacitors and inductors loading," in *2024 IEEE 12th Asia-Pacific Conference on Antennas*

and Propagation (APCAP), 1–2, Nanjing, China, 2024.

[13] Narayane, V. B. and G. Kumar, "A selective wideband bandpass filter with wide stopband using mixed lumped-distributed circuits," *IEEE Transactions on Circuits and Systems II: Express Briefs*, Vol. 69, No. 9, 3764–3768, 2022.

[14] Luo, X., S. Sun, and R. B. Staszewski, "Tunable bandpass filter with two adjustable transmission poles and compensable coupling," *IEEE Transactions on Microwave Theory and Techniques*, Vol. 62, No. 9, 2003–2013, 2014.

[15] Zhu, L., S. Sun, and R. Li, *Microwave Bandpass Filters for Wideband Communications*, John Wiley & Sons, 2011.